Compartmentalized nanoparticles in aqueous solution through hierarchical self-assembly of triblock glycopolymers

Journal:	*Polymer Chemistry*
Manuscript ID	PY-ART-05-2018-000792.R1
Article Type:	Paper
Date Submitted by the Author:	05-Jul-2018
Complete List of Authors:	Piloni, Alberto; University of New South Wales, School of Chemistry Walther, Andreas; University of Freiburg, Institute for Macromolecular Chemistry Stenzel, Martina; University of New South Wales, School of Chemistry

Polymer Chemistry

PAPER

Compartmentalized nanoparticles in aqueous solution through hierarchical self-assembly of triblock glycopolymers†

Received 00th January 20xx,
Accepted 00th January 20xx

DOI: 10.1039/x0xx00000x

www.rsc.org/

Alberto Piloni, [a] Andreas Walther*[b,c,d,e] and Martina H. Stenzel*[a]

Amphiphilic block copolymers can elegantly assemble in water to form well-defined nano-objects and through smart design or the polymers it is possible to efficiently prepare functional materials for biomedical applications such as drug carriers. Linear triblock terpolymers add an additional level of complexity to the process. The assembly can proceed in a step-wise manner, collapsing one block at a time and producing materials with segregated domains in the nanometer scale. Here we present the self-assembly of a pH-responsive and sugar-functionalized linear triblock terpolymer PGlcEA-*b*-PBuA-*b*-P4VP in aqueous solution. Initially the polymer forms small spherical micelles with a poly(butylacrylate) core and a corona composed by the two outer blocks. Subsequent exchange of the solvent to aqueous solution at different pH value causes aggregation into bigger particles triggered by the segregation of the poly(4-vinylpyridine) block. Morphologies include large patchy spherical particles and caterpillar-type structures and are strongly influenced by the acidity of the solution. We determine the best conditions for the preparation of the aggregates and study their stability to ageing and temperature variation with particular focus on the "caterpillars". Our results demonstrate that a hierarchical self-assembly can be useful to expand the morphological diversity of polymeric nanoparticles in aqueous solution bearing bioactive surface functionalities.

Introduction

Self-assembly of block copolymers continues to attract considerable attention for the bottom-up design of nanomaterials in solution. Using a simple solvent exchange process, it is possible to trigger microphase-separation via selective solvation, allowing the formation of stable and narrowly dispersed polymer particles ranging from tens to hundreds of nanometers in size. Progress in polymerization techniques and ease of functionalization have advanced the preparation of polymers with precise composition and architecture, leading to self-assembled particles with a wide variety of chemical and physical properties.[1-4] The potential of this method has been recognized most notably in the biomedical field for the preparation of nanocarriers consisting of a hydrophilic corona and a hydrophobic core that can be used to encapsulate therapeutic drugs and enable their delivery to a target tissue, in particular by embedding biological epitopes into the particle shell.[5] Spherical core/shell particles and vesicular structures have received the most widespread attention as they are the most easily accessible ones using AB linear block copolymers. The preparation of rods, on the contrary, requires careful tuning of polymer composition and self-assembly procedures and can result in kinetically trapped structures.[6, 7]

[a] Centre for Advanced Macromolecular Design, School of Chemistry, UNSW, Sydney, NSW 2052, Australia
[b] Institute for Macromolecular Chemistry, Stefan-Meier-Strasse 31, University of Freiburg, 79104 Freiburg, Germany
[c] Freiburg Materials Research Center, Stefan-Meier-Strasse 21, University of Freiburg, 79104 Freiburg, Germany
[d] Freiburg Center for Interactive Materials and Bioinspired Technologies, Georges-Köhler-Allee 105, University of Freiburg, 79110 Freiburg, Germany
[e] Freiburg Institute for Advanced Studies, University of Freiburg, 79104 Freiburg, Germany

†Electronic Supplementary Information (ESI) available: NMR, DLS, TEM. See DOI: 10.1039/x0xx00000x

The self-assembly of more complex architectures, such as multiblock linear polymers or miktoarm star polymers, has received growing interest because it allows access to a wider array of morphologies.[8-10] With more than two chemically different environments connected to each other it is possible to prepare multicompartment micelles, consisting of segregated core domains.[11] Examples include spherical,[12-15] linear[16] and more complex structures.[17] Intrinsic chemical incompatibility is the driving force causing the core-forming blocks to form segregated domains, for instance a lipophilic and fluorophilic compartment.[12-14] In a more elaborate process, it has been shown that highly ordered and well defined compartmentalized structures can be obtained with linear block terpolymers by triggering a change in solubility of one block at a time as opposed to a one-step assembly. The terpolymers initially form primary particles acting as building blocks for a more complex aggregates. Systematic experimentation using libraries of block terpolymers have identified some of the factors influencing the self-assembly and established a theoretical framework to predict the morphology of the aggregate depending on the volume ratio of the core forming blocks and the swelling of the corona.[18, 19] Tailoring of this ratio can be achieved either by different degree of polymerization or modulating solvent composition to cause swelling or contraction of one of the compartments. These detailed studies show that the self-assembly behavior of such block terpolymers can be highly predictive.

Techniques to reliably tune the nanoparticle shape are of great interest in drug delivery. It has been demonstrated that morphology, as well as size, can influence cellular uptake and circulation time. Elongated or flat nano-objects have a different flow behavior compared to spherical particles and can bind more effectively onto the cellular membrane, increasing the rate of endocytosis.[20, 21] The filamentous shape and the highly ordered surface structure of viruses like ebola influence their ability to penetrate the cellular membrane.[22] We can draw inspiration from these efficient pathogens in the design of synthetic drug carriers.

Unfortunately, most of the work on compartmentalized nanoparticles has focused exclusively on organic solvents and their mixtures, whereas it is of key importance to bring this conceptual methodology to aqueous media to target applications in the biomedical field. To trigger compartmentalization of triblock terpolymers in water, thermoresponsive[23-25] and pH-responsive[26, 27] segments have been employed. PNiPAM causes reversible aggregation between particles by increasing and lowering the temperature depending on the polymer length.[23] In another contribution, poly(4-vinyl pyridine) (P4VP) was used in different block terpolymer architectures to produce particles with a patchy surface derived from compartmentalization.[28-30] While these studies demonstrate that a stepwise assembly is possible in aqueous solutions, the morphological variety is not as broad and predictable as reported for more simple systems, and critically, also often suffers from higher dispersity than in organic solvents.

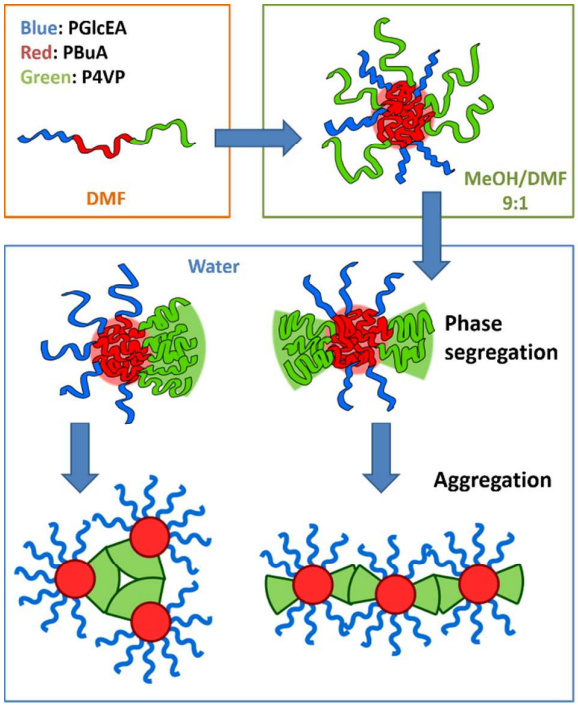

Fig. 1 Schematic representation of hierarchical self-assembly of the triblock terpolymers upon step-wise structure formation. Addition of methanol causes the collapse of the central PBuA block (red) forming spherical core/shell micelles. Dialysis against water triggers segregation of the P4VP domain (green) and, depending on the pH of the solution, aggregation between particles produces compartmentalized structures. The PGlcEA block (blue) is always soluble and constitutes the hydrophilic corona.

A step forward was recently achieved with a promising terpolymer system containing both a bioactive glycopolymer block and a pH-responsive P4VP block. Particle formation under different acidity produced patchy spherical aggregates and elongated structures with alternating domains.[31] Since glycopolymers have emerged as interesting candidates for the surface composition of nanocarriers,[32, 33] it is important to gain deeper understanding of the hierarchical self-assembly of these triblock terpolymers in water.

Here we elucidate the self-assembly behavior of a linear pH-responsive PGlcEA-*b*-PBuA-*b*-P4VP triblock terpolymer in aqueous solution. The polymer is designed with a hydrophobic and low T_g PBuA central block, a hydrophilic and bioactive glucose-functionalized block (PGlcEA) and a pH-switchable P4VP block to direct the self-assembly. A hierarchical process outlined in Fig. 1 is followed and the control over the final morphology is achieved by fine-tuning the volume of the pH-responsive block, changing the degree of ionization and ultimately affecting solubility in water. We show that at different pH, the P4VP block can trigger hierarchical self-assembly from core/shell spherical micelles to different nanoparticles with a phase-segregated core and interesting morphologies, such as patchy micelles and “caterpillar” shapes with alternating domains. Aggregation between micelles rather than just collapse of the P4VP domain within the same particle, is the mechanism producing the morphological variety

in agreement with hierarchical self-assembly studies in organic solvents.[18] The effect of the degree of ionization, time, temperature and concentration is explored to evaluate the thermodynamic stability of the aggregates, clearly highlighting the occurrence of metastable areas.

Experimental

Materials

Tripotassium phosphate (K_3PO_4), 3-mercaptopropionic acid, carbon disulfide, benzyl bromide, sodium acetate, acetic anhydride, D-glucose, 2-hydroxyethyl acrylate (HEA), boron trifluoride diethyl etherate, sodium bicarbonate, sodium methoxide, methyl iodide, monopotassium phosphate (KH_2PO_4), hydrochloric acid and sodium hydroxide were purchased from Sigma-Aldrich and used as received. Dimethylsulfoxide-d6 and deuterated chloroform were purchased from Cambridge Isotope Laboratories. n-Butyl acrylate (BuA) and 4-vinyl pyridine (4VP) were purchased from Sigma-Aldrich and filtered over basic aluminium oxide before use. 2,2'-Azobis(2-methylpropionitrile) (AIBN) was purchased from Sigma-Aldrich and recrystallized from methanol before use.

Analyses

FT-NIR Spectroscopy. A Bruker IFS\S Fourier transform spectrometer was used for the measurements, with a tungsten halogen lamp, a CaF_2 beam splitter and a liquid nitrogen cooled InSb detector. The spectral region of interest was between 7000 and 5000 cm^{-1} with a resolution of 4 cm^{-1}. Using a heating block the sample was maintained at 70 ± 0.5°C.

Nuclear Magnetic Resonance (NMR). Either a Bruker Avance III 300 MHz, 5 mm BBFO probe (^{1}H: 300.17 MHz) or a Bruker Avance III HD 400 MHz, 5 mm BBFO probe (^{1}H: 400.13 MHz) spectrometer were used for NMR measurements. Solvents employed were $CDCl_3$, DMSO-d_6 and MeOD-d_4 and chemical shifts are expressed in ppm relative to residual solvent peaks. Measurements were performed at 25°C unless otherwise stated. The raw data was processed using Bruker TOPSPIN 3.2 software.

Size Exclusion Chromatography (SEC). Experiments were run on a Shimadzu modular system with SIL-10AD autoinjector, LC-10AT pump, CTO-10A oven, 5.0-µm bead guard column (50 x 7.8 mm) followed by four 300 x 7.8 mm linear columns with 500, 103, 104, 105 Å pore size and 5 µm particle size. The solvent system was N,N-dimethylacetamide (HPLC grade) with 0.05% w/v 2,6-dibutyl-4-methylphenol and 0.03% w/v LiBr. Flow rate was 1 mL/min at 50°C and a refractive index detector was used (Shimadzu RID-10A). The calibration was performed using narrow polydispersity PMMA standards (0.5−1000 kDa) purchased from Polymer Laboratories.

Dynamic Light Scattering (DLS). A Malvern Zetasizer equipped with a He-Ne laser (4 mV) operating at 632 nm was used and the detection was at 173°.

Transmission Electron Microscopy (TEM). A JEOL1400 TEM operating at 100 and equipped with a Gatan CCD camera was used. Samples were deposited on a 200 mesh copper grids coated with Formvar and carbon. 5 µL of sample at a concentration ranging from 1 to 0.1 mg/mL were deposited on the grids. After 2 min the excess liquid was blotted away and the grid was air dried for at least one hour. If desired, a 2 wt. % solution of uranyl acetate in water was used to stain the samples for 5 min.

Turbidimetry ConA Binding Assay. Measurements were performed on a Cary 60 UV-vis spectrometer. A ConA solution (0.5 mg/mL) in sodium acetate/acetic acid buffer (5mM) was prepared and 3 mL were transferred in a glass UV-vis cuvette. The solution was used as baseline. 20 µL of nanoparticle sample (1 mg/mL) was added to the cuvette a time dependent absorption measurement at 420 nm was started immediately for 10 min.

Syntheses

Synthesis of 3-(benzylthiocarbonothioylthio)propionic acid (BSPA) RAFT agent. The compound was synthesized as previously reported.[34] Tripotassium phosphate (1.8 g, 8.48 mmol) was suspended in 20 mL of dry THF and 1.00 mL (7.74 mmol) of 3-mercaptopropionic acid was added. The suspension was left stirring for 10 minutes and cooled down to 0°C. Carbon disulfide (1.40 mL, 23.2 mmol) was added dropwise and the resulting yellow solution was stirred for two hours at room temperature. Dropwise addition of benzyl bromide (0.92 mL, 7.74 mmol) caused precipitation of KBr as a white powder and the reaction mixture was stirred for 15 hours. The salt was removed by filtration and the solvent evaporated to afford a yellow oil. Approximately 20 mL of MilliQ water were added and the product was extracted with dichloromethane (3x40 mL). The combined organic phase was washed with brine (3x50 mL), dried over magnesium sulfate and the solvent was removed under reduced pressure. The crude yellow solid was purified by crystallization: after dissolution in approximately 5 mL of DCM, n-hexane was added dropwise until the solution turned slightly cloudy. After refrigeration at 4°C overnight the needle-like yellow crystals were collected by vacuum filtration, washed with cold n-hexane and air dried (yield: 1.60 g, 76%). ^{1}H NMR (300 MHz, $CDCl_3$) δ_H = 9.10-10.40 (1H, br s, COO*H*), 7.26-7.36 (m, 5H, Ph), 4.62 (s, 2H, S-C*H*2-Ph), 3.62 (2H, t, S-C*H*2-CH2, *J* = 7 Hz), 2.85 (t, 2H, S-CH2-C*H*2, *J* = 7 Hz).

Synthesis of 1,2,3,4,6-penta-O-acetyl-β-D-glucopyranose (AcGlc). As per literature[32], a suspension of sodium acetate (7.7 g, 93.3 mmol) in acetic anhydride (80 mL) was heated up to 120°C. D-Glucose fine powder was added (15.0 g, 83.3 mmol) and the mixture turned pale pink. After 30 minutes the solution was poured into 500 mL of ice-cold deionized water causing the acetylated sugar to precipitate as a white powder. The precipitate was recovered by suction filtration and washed with cold water. Recrystallization was performed from approximately 200 mL of boiling ethanol. After refrigeration at 4°C for about 2 hours the product was collected as a white solid by filtration (yield: 18.1 g, 56%). ^{1}H NMR (300 MHz, $CDCl_3$) δ_H = 5.71 (1H, d, *J* = 7 Hz), 5.25 (1H, t, *J* = 9 Hz), 5.09-5.15 (2H, m), 4.07-4.32 (2H, m, CH_2), 3.84 (1H,

m), 2.11 (3H, s, CH_3), 2.08 (3H, s, CH_3), 2.03 (3H, s, CH_3), 2.01 (3H, s, CH_3).

Synthesis of 2-(2',3',4',6'-tetra-O-acetyl-D-glucosyloxy) ethyl acrylate (AcGlcEA). Following a modified literature procedure[35], 8 g (20.5 mmol) of acetylated glucose (AcGlc) were dissolved in anhydrous dichloromethane (100 mL). 2-Hydroxyethyl acrylate (HEA) was then added (26.7 mmol) and the solution was cooled down to 0°C. Under nitrogen flow boron trifluoride diethyl etherate (8.9 mL, 71.8 mmol) was added dropwise over a period of 30 minutes. The reaction was carried out at room temperature for 20 hours. The yellowish solution was poured into 150 mL of ice-cold deionized water and the crude product was extracted with DCM (2x50 mL), washed with 100 mL of saturated sodium bicarbonate solution and 100 mL of brine. The organic phase was dried over magnesium sulfate and the solvent was evaporated under reduced pressure obtaining the crude product as a pale yellow oil. Purification by column chromatography was carried out using a 2:3 mixture of n-hexane and ethyl acetate yielding 3.26 g of colorless oil (36%). ^{1}H NMR (300 MHz, $CDCl_3$) (Fig. S1†) δ_H = 6.42 (1H, d, J = 17 Hz, CH_2-CH), 6.13 (1H, dd, J = 17, 10 Hz, CH_2-CH-C), 5.85 (1H, d, J = 10 Hz, CH_2-CH), 5.42 (1H, t, J = 9 Hz, CH-CHO-CH), 5.24 (1H, m, CH-CHO-CH), 5.04 (1H, dd, J = 9, 7 Hz, CH-CHO-$CH_{anomeric}$), 4.56 (1H, d, J = 7, O-C$H_{anomeric}$O-CH), 3.82-4.35 (7H, m, CH_2), 2.17 (3H, s, CH_3), 2.07 (3H, s, CH_3), 2.05 (3H, s, CH_3), 2.01 (3H, s, CH_3).

Synthesis of poly(2-(2',3',4',6'-tetra-O-acetyl-D-glucosyloxy) ethyl acrylate (PAcGlcEA). RAFT polymerization was employed for the synthesis. AcGlcEA (640 mg, 1.43 mmol), BSPA RAFT agent (3.9 mg, 0.014 mmol) and AIBN initiator (0.23 mg, 0.0014 mmol) were dissolved in 1.2 mL of toluene. The mixture was transferred into a sealed FT-NIR glass cuvette and purged with nitrogen for 20 minutes. The polymerization was carried out at 70°C and monomer conversion was monitored by IR measuring the integral of the vinylic peak over time (Fig. S2†). The reaction was interrupted after 5 hours by cooling down the mixture to 0°C and introducing air. The ^{1}H NMR spectrum of the crude polymerization was used to calculate monomer conversion (60%) and theoretical molecular weight comparing the ratio between monomer and polymer peaks. The polymer was purified by precipitation in cold diethyl ether (40 mL) and dried in vacuo obtaining a yellow glassy solid.

Chain extension of macro RAFT PAcGlcEA with n-butyl acrylate (PAcGlcEA-PBuA). The purified macro RAFT agent PAcGlcEA (250 mg, 0.0093 mmol), n-butyl acrylate (0.400 mL, 2.78 mmol) and AIBN initiator (0.152 mg, 0.000926 mmol) were dissolved in toluene (1.5 mL). The mixture was transferred into a sealed FT-NIR glass cuvette and purged with nitrogen for 20 minutes. The polymerization was carried out at 70°C in an IR spectrometer for 1.5 hours (Fig. S2†). The reaction was stopped by cooling down the mixture to 0°C and introducing air. Monomer conversion (65 %) and theoretical molecular weight were calculated by ^{1}H NMR and the polymer was precipitated twice in cold n-hexane (50 mL). The resulting sticky yellow solid was dried under vacuum.

Chain extension of diblock macro RAFT PAcGlcEA-PBuA with 4-vinyl pyridine (PAcGlcEA-PBuA-P4VP). The diblock PAcGlcEA-PBuA macro RAFT (160 mg, 0.0030 mmol) was dissolved in N,N-dimethylacetamide (1.5 mL) together with 165 µL of 4-vinyl pyridine (158 mg, 1.5 mmol) and 0.10 mg of AIBN initiator (0.0006 mmol). The pale yellow solution was degassed by three freeze-pump-thaw cycles and reacted under nitrogen atmosphere in a pre-heated oil bath at 70°C for 20 hours. The polymerization was stopped cooling the solution with ice and introducing air. ^{1}H NMR was used to calculate the conversion (32%) and the theoretical molecular weight.

Deprotection of the triblock terpolymer (PGlcEA-PBuA-P4VP). Deacetylation of the glucose moieties was performed directly on the crude polymerization. The solution was diluted with 8 mL of methanol/chloroform 1:1 mixture. 0.4 mL of 2.5 wt. % solution of sodium methoxide in methanol were added dropwise under vigorous stirring (0.18 mmol of sodium methoxide). After 1 hour the solution was concentrated to remove most of the chloroform and was dialyzed against milliQ water for 24 hours. The polymer was recovered by lyophilization as a white solid and characterized by NMR at 60°C (Fig. S3†).

Post-polymerization methylation of P4VP. 5 mg of deprotected triblock terpolymer were dissolved in 600 µL of DMSO-d6 and 10 µL of methyl iodide (10 eq. per pyridine unit) were added to the solution. The reaction was stirred at room temperature for one hour and ^{1}H NMR of the crude confirmed successful methylation of the pyridine functionality (Fig. S4†). The solution was diluted with 2 mL of methanol and dialyzed against water for 24 hours changing the solvent after the first 4 hours. The product was recovered by lyophilization (3.9 mg).

Self-assembly

General procedure of self-assembly of triblock terpolymer into core-shell micelles. Typically 2 mg of triblock terpolymer were dissolved in 200 µL of DMF. Stirring and heating gently with a heat gun (100°C) for a couple of minutes helped the dissolution. To the well stirred solution 1.8 mL of methanol were added dropwise over a period of approximately 20 minutes to form core-shell micelles. The colloidal solution was sealed and annealed overnight at 50°C. After cooling to room temperature the sample was characterized with DLS.

General procedure of self-assembly of core-shell micelles into higher level aggregates in aqueous solution. The 1 mg/mL solution in methanol/DMF 9:1 obtained in the previous step was used as a starting point. In dilution experiments an appropriate volume of methanol was added to obtain the desired concentration. Typically, 200 µL were then transferred in a 3500 MWCO dialysis bag and dialyzed against 1 L of aqueous solution of certain pH or buffer strength for about 20 hours.

RESULTS AND DISCUSSION

Block copolymer design and synthesis

Our rationale for the design of the ABC triblock terpolymer starts with having two water-soluble outer blocks, PGlcEA and P4VP, separated by a lipophilic central block (PBuA). While the glucose-bearing PGlcEA is water-soluble at any condition, the hydrophilicity of P4VP can be tuned with the pH value. The pH-responsiveness of P4VP will later be used to trigger rearrangements of the corona and formation of compartmentalized particles as schematically shown in Fig. 1. The central block is long and hydrophobic to account for the folding necessary to form core/shell micelles exposing both terminal blocks. Targeting a P4VP block length just below the PBuA ensures that a change in external conditions can tune the volume so that $V_{PBuA}>V_{P4VP}$ for a completely deprotonated state and $V_{PBuA}<V_{P4VP}$ for a protonated, swollen state. This follows the rationale that changes in volume ratios can stir the hierarchical self-assembly towards different morphologies.[18]

this protected form in toluene. After chain extension with BuA and 4VP we proceeded to deacetylate the sugar side-chains restoring hydrophilicity of the first block. A diluted solution of sodium methoxide was used to avoid cleavage of the side chain and NMR confirmed deprotection with negligible loss of sugar moieties (Fig. S3†). Time-dependent FTIR spectroscopy (Fig. S2†) and ^{1}H NMR were used to monitor conversion during and after the polymerizations. Size exclusion chromatography (SEC) analysis after each polymerization step shows a clear shift of the molecular weight distribution, demonstrating good chain extension. Tailing, broadening and non-symmetric distributions indicate the presence of a small amount of remaining homopolymer and diblock copolymer in the mixture (Scheme 1). Even though this will affect the theoretical ratio between the blocks, we do not expect it to have a strong effect on the self-assembly. Purification by dialysis and lyophilization

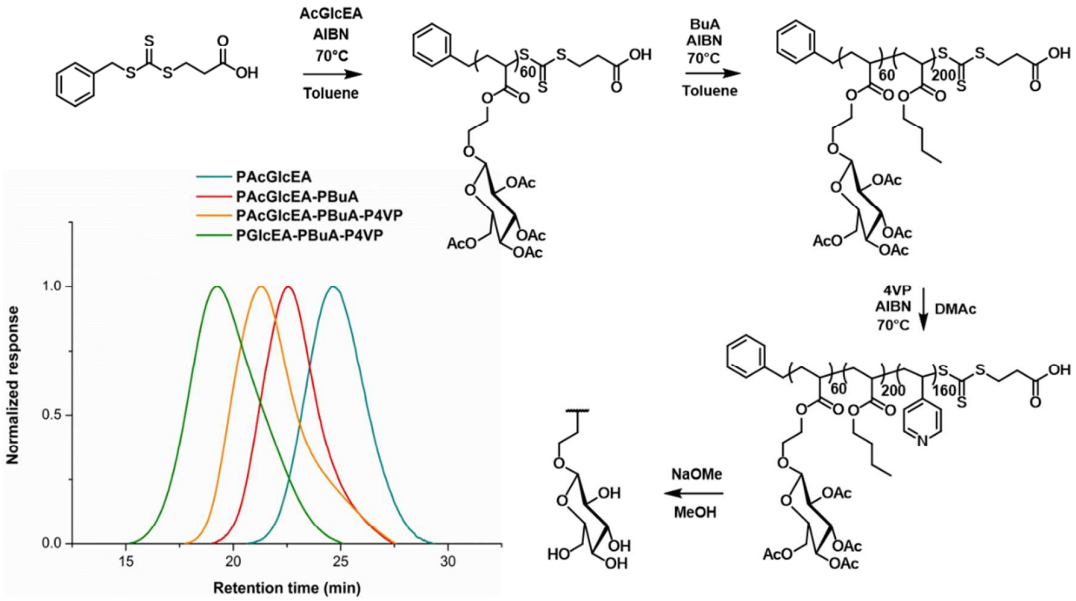

Scheme 1 Synthesis of linear triblock terpolymer PGlcEA-*b*-PBuA-*b*-P4VP. Three consecutive RAFT polymerizations were performed, followed by deacetylation of the sugar block. SEC curves obtained in DMAc.

We used three consecutive RAFT polymerizations using 3-(benzylthiocarbonothioylthio)propionic acid (BSPA) as CTA and AIBN as thermal initiator to synthesize the well-defined ABC triblock terpolymer (Scheme 1). A trithiocarbonate chain transfer agent was chosen to allow controlled polymerization of both acrylates and styrenic monomers.[4] Following a modified literature procedure outlined in Scheme S1† we synthesized a tetra-acetylated version of the glucose-functionalized acrylate[35] and carried out the polymerization in

yields the $PGlcEA_{60}$-*b*-$PBuA_{200}$-*b*-$P4VP_{160}$ triblock copolymer ($M_{n,\,theo}$ = 59,400 g/mol) with the desired amphiphilic and pH-responsive properties (Table 1). The disagreement between theoretical and experimental molecular weight average can be attributed to the calibration standards (PMMA) and is often observed in the case of polymers with bulky side chains. In particular the deacetylated glycopolymer has a larger SEC elution volume than the protected precursor. In the self-assembly study, we exploit the characteristic solubility of

each block and the low T_g of the middle PBuA block to direct the arrangement of polymer chains upon solvent exchange.

Formation of core/shell micelles

After preparation of the triblock terpolymer, we studied the self-assembly behavior under different conditions. Following a step-wise process, the polymer was first dissolved in dimethylformamide (DMF), a good solvent for all three blocks. Dynamic light scattering (DLS) indicates dissolution of the polymer on a molecular level and absence of any aggregation. Methanol is a suitable solvent for primary particle formation as it can dissolve both P4VP and PGlcEA blocks, while being a poor solvent for PBuA. Indeed, after dropwise addition under fast stirring, micelles are formed with a PBuA core and a shell, most probably composed of mixed P4VP and PGlcEA chains.

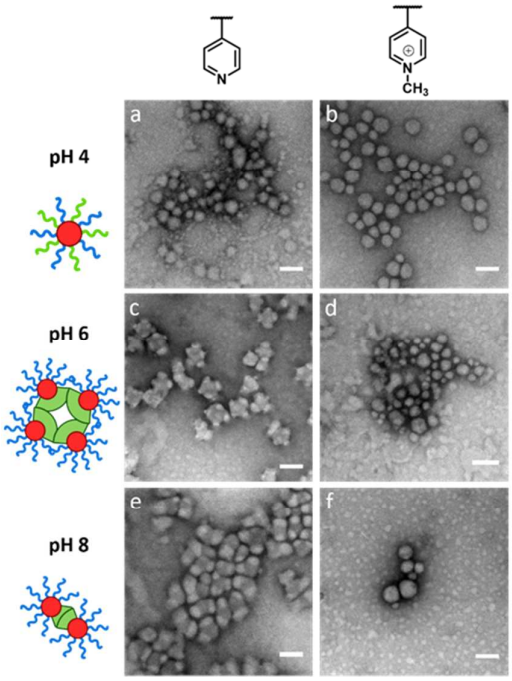

Fig. 2 TEM micrographs of self-assembled particles formed in milliQ water. Different structures are shown at a pH of approximately 4 (a), 6 (c) and 8 (e) for the P4VP containing terpolymer while only spherical micelles were formed when the pyridine functionality is quaternized (b, d, f). All samples are stained with uranyl acetate to improve contrast especially in case of spherical particles. Scale bars are 100 nm. Additional unstained images can be found in Fig. S6†.

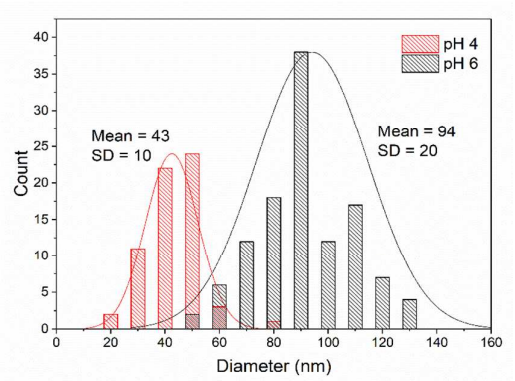

Fig. 3 Size distribution of the cores of the aggregates formed by PGlcEA-b-PBuA-b-P4VP in milliQ water. A significant difference in size between pH ≈ 4 and pH ≈ 6 confirms that the pH-responsiveness of P4VP can trigger aggregation between primary particles as the pH increases. Obtained from statistical image analysis of TEM images.

The z-average hydrodynamic diameter obtained by DLS right after addition is $\langle D_h \rangle_z$ = 103 nm ($Đ$ = 1.14), but annealing the colloidal solution at 50°C for about 20 hours allows the micelles to reach near-equilibrium conformation with a $\langle D_h \rangle_z$ = 74 nm and low dispersity $Đ$ = 1.09 (Fig. S5†). This micellar size in solution is within the expected value in the model in which the polymer has a partially extended corona block ($P4VP_{160}$ < 48 nm in length) and a folded middle block in the core ($PBuA_{200}$ < 30 nm). The micelles are highly stable in methanol/DMF 9:1 mixtures and no change in the diameter or count rate can be observed up to four weeks after preparation. These primary particles represent the starting point of all following self-assembly experiments and their aggregation behavior upon switching to aqueous environment determines the morphology of the final product. Consistently with hierarchical self-assembly literature[18] we found low dispersity of primary building blocks to be crucial to achieve ordered aggregation on the next level.

Self-assembly in deionized water

Dialysis of the MeOH/DMF dispersion of core/shell micelles (our primary particles) against deionized water triggers the higher-level self-assembly. Fig. (a,c,e) show TEM micrographs of three different morphologies. Dialysis against acidic water (pH ≈ 4, adjusted with 1M HCl) produces only small spherical

Table 1. Summary of the characterization of the polymers.

Polymer	DP[a]	M_n (theo)[a] [g/mol]	SEC[b]	
			M_n [g/mol]	$Đ$
PAcGlcEA	60	27,000	15,400	1.39
PAcGlcEA-*b*-PBuA	60-200	52,600	32,300	1.23
PAcGlcEA-*b*-PBuA-*b*-P4VP	60-200-160	69,400	41,200	1.43
PGlcEA-*b*-PBuA-*b*-P4VP	60-200-160	59,400	82,100	1.29

[a] Obtained by ^{1}H NMR of the polymerization mixture comparing the integrals of the peaks belonging to the polymer and the leftover monomer. [b] SEC in DMAc

particles with no evidence of clear phase separation or aggregation, indicating a mixed PGlcEA/P4VP shell (Fig. a). This behavior is consistent with a highly ionized and hydrophilic P4VP block, which wants to occupy the whole shell due to electrostatic repulsion between the chains. On the contrary, dialysis against basic water (pH ≈ 8, adjusted with 1M NaOH) causes the deprotonated P4VP block to segregate and form a separate core compartment. Since the pK_a of P4VP is reported to be around 5,[36] the degree of ionization of this block under these conditions is minimal and water solubility is strongly reduced. The resulting nanoparticles have a P4VP compartment (dark) capped by two PBuA compartments on each side (light) as shown in Fig. e. This behavior is the result of the aggregation of two or three primary particles joining their now insoluble P4VP blocks to maintain colloidal stability. Neutral milliQ water also produces compartmentalized aggregates. In this case the number of aggregating primary particles is higher and patchy spheres with a common P4VP central compartment (dark) and three or more PBuA patches (light) can be observed (Fig. c). Statistical analysis of the approximate TEM diameter of the cores of the aggregates at pH 6 (D_n = 94 nm) confirms a significant increase in size compared to pH 4 (D_n = 43 nm). This increase suggests that compartmentalization of the P4VP block is indeed followed by aggregation between primary particles (Fig.). Dynamic light scattering gives somewhat conflicting results, with the highest size and dispersity for the acidic sample (Table S1†). We presume that measurements in milliQ water of the colloidal solutions could be influenced by long range particle interactions and give an artificially large hydrodynamic diameter. This hypothesis is confirmed by following experiments in which low concentration buffer solution were used.

To confirm that the pH-dependent aggregation behavior arises from the pH-responsive solubility of the P4VP block, we explored the self-assembly of a methylated version of the polymer after full quaternization of the P4VP block (^{1}H NMR in Fig. S4†). This post-polymerization modification approach allows comparing two polymers with identical composition, but different response towards pH change. The same solvent exchange procedure was used for the self-assembly and, as expected, TEM only depicts spherical micelles at pH 4, 6 and 8 with similar low diameters (Fig. b, d, f). Since a permanently charged QP4VP block does not exhibit any pH-dependent water solubility, such block always constitutes the hydrophilic corona and phase segregation does not occur at any pH value, leading to similar morphologies during transfer into water. This is also corroborated by DLS (Table S1†) showing consistent value of the micelle in the range of 89-117 nm, corresponding to the primary particle in MeOH/DMF 9:1 with a slight expansion in water due to the higher dielectric constant.

Self-assembly in aqueous buffers

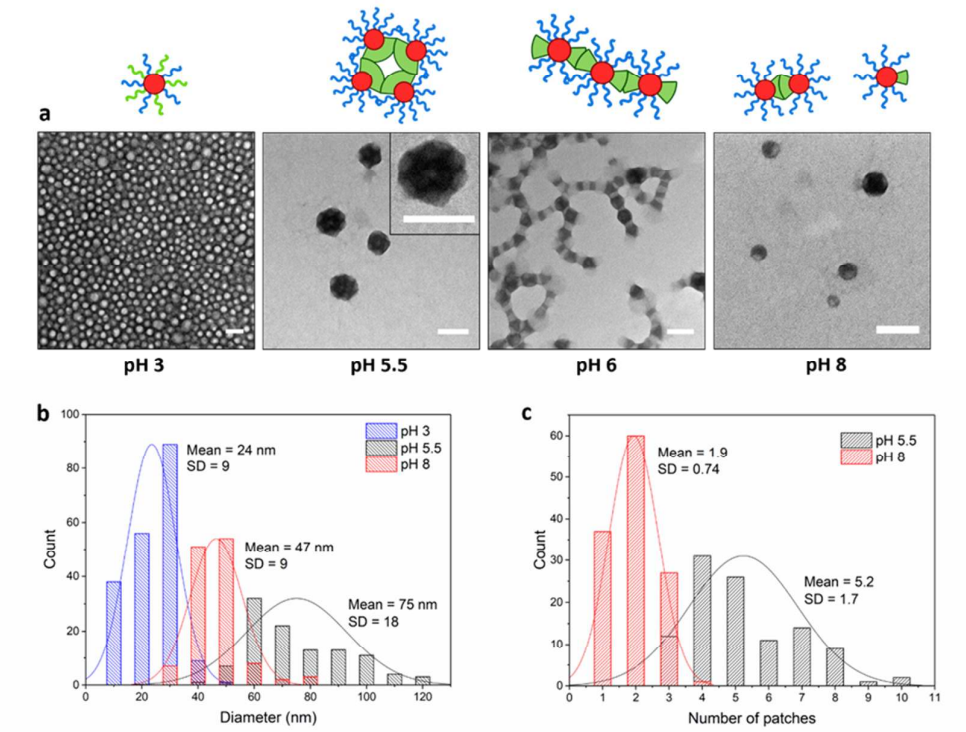

Fig. 4 Self-assembly of PGlcEA-b-PBuA-b-P4VP in buffer solutions. (a) Representative TEM micrographs of particles obtained after dialysis against buffer solution (5 mM) at different pH values showing different morphologies. (b) Size distribution of the aggregate cores and (c) number of patches shows a significant difference in the aggregation behavior. Additional images in Figure S7† (first column). Scale bars are 100 nm.

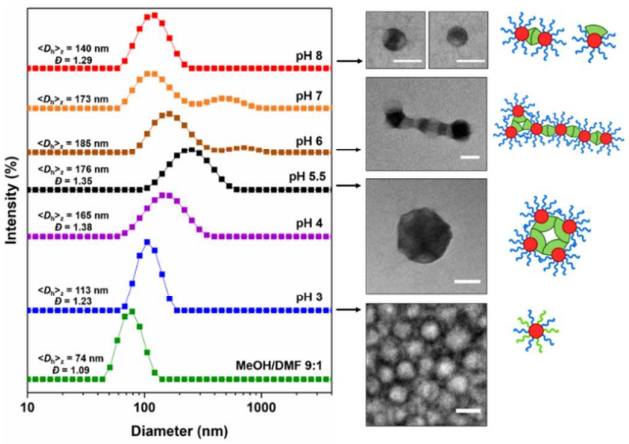

Fig. 5 Hydrodynamic diameter by DLS before and after dialysis against 5 mM buffer. TEM images are representative of the morphology under different conditions. At low pH the highly protonated P4VP block shares the corona with the PGlcEA block, at moderate to high pH the degree of protonation determines the volume of the segregated P4VP domain and influences both size and number of PBuA patches of the final aggregate. Only at pH 6 "caterpillars" can be accessed. Scale bars are 50 nm.

While the system clearly shows a pH responsiveness and a tendency to form segregated core domains, the use of unbuffered aqueous solutions prevents us from accurately controlling the degree of ionization of the P4VP block. To fully monitor the aggregation behavior at specific pH values we next employ commonly used buffers and characterize the particles by TEM (Fig. a, Fig. S7†) and DLS (Fig. , Table S2†). Sodium acetate/acetic acid buffer solutions (5 mM) were used for dialysis against up to pH 6, while K_2HPO_4/KH_2PO_4 solutions were used for higher pH values. Acidic environments (pH 3 and 4 corresponding to > 90% ionization of the P4VP) only lead to small spherical particles, consistently with the case of the unbuffered solution, due to the high solubility of the highly protonated P4VP block. The particles maintain the same morphology as in methanol/DMF. At pH 5 (50% ionization) and above, a range of compartmentalized aggregates form due to the partial deprotonation and collapse of the P4VP block. The most common morphology is the "patchy spherical" one observed in many of the TEM micrographs (Fig. S7†). The patchy appearance is once again due to the separation between PBuA (light) and P4VP (dark) domains in the core of the nanoparticles. The increase in size can also be observed on DLS as shown in Fig. . pH values of 6.5 and above (<3% ionization) show a predominance of smaller patchy aggregates consisting of only two or three primary micelles. Some Janus type spherical particles, with only one PBuA domain, can also be observed at pH 7 and 8. They are caused by the significant shrinkage of the P4VP compartment at less than 1% ionization, whereby aggregation is avoided due to the hydrophilic PGlcEA corona. DLS measurements in Fig. (and Table S2†) often show a larger diameter than TEM micrographs (Fig. b). The difference can be attributed to two factors. Since the particles in solution have a bulky hydrated corona, the hydrodynamic size appears larger than the dry particles deposited for imaging. Secondly, in case of non-stained samples, only the dark P4VP-rich core can be seen on the TEM micrographs. Nevertheless we can see a trend in the hydrodynamic size distribution that informs us on the aggregation state of the colloidal solutions.

An interesting aggregation behavior can be observed at pH 6 (Fig. a). The primary particles line up forming "caterpillars" in which the P4VP (dark) and PBuA (light) domains alternate in a linear or branched structure. To access this morphology the P4VP block in the primary particles must segregate in two distinct domains on opposite sides of the PBuA core to form building blocks with "sticky" caps that will direct aggregation into linear structures rather than spherical ones (Fig. 1). This behavior occurs for both sodium acetate and phosphate buffer (Fig. S7†), indicating that the effect of the counterion on the assembly is limited. 5 mM buffers allow us to maintain a constant pH value while disregarding the effect of salt concentration during self-assembly. Since biological applications often require a higher concentration, we evaluated the stability of the solution at pH 6 and 8 using DLS (Table S3†). Increasing the buffer concentration by addition of an appropriate volume of 100 mM buffer solution has little effect on the size distribution up to 37 mM. Dialysis of the primary particles against 100 mM buffer, on the contrary, causes precipitation of the polymer. This indicates that high salt concentration can affect the colloidal stability of the particles.

Effect of ageing and annealing

The narrow window for observation of the caterpillar-type structures prompted us to assess the thermodynamic stability of the colloidal solutions by ageing the samples for three days at 25 °C or annealing them at 45 °C for one day. Indeed, ageing and annealing affect the morphology distribution. "Caterpillar" aggregation behavior at pH 6 is strongly reduced after annealing at 45 °C and spherical aggregates become more prominent at intermediates pH values (6 – 7), while spherical morphologies at high and low pH undergo little to no change (Fig.). The effect is less pronounced, yet still clearly visible, after letting the dispersion age at room temperature for three days (Fig. S7†). This behavior suggests that the "patchy spherical" morphology is the thermodynamically stable one when the P4VP block is deprotonated and the PBuA core is given sufficient time and/or energy to reorganize the internal structure.

Capturing caterpillars

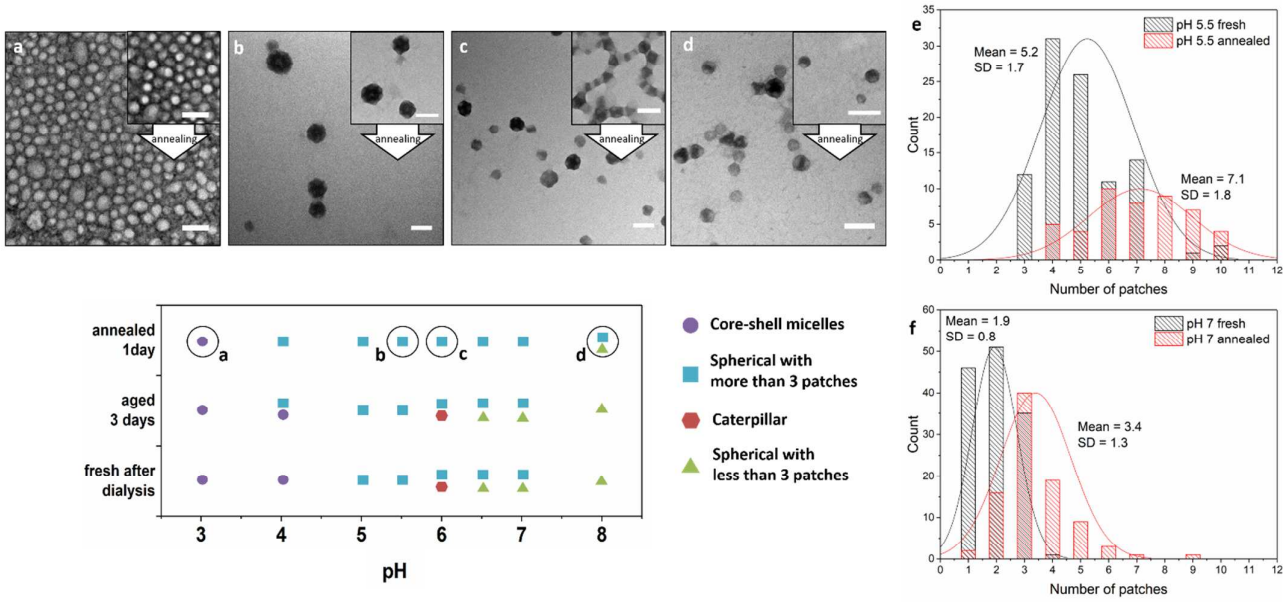

Fig. 6 Effect of annealing of the colloidal solution in 5mM buffer. The diagram summarizes the predominant morphology observed from TEM images under the condition specified. All samples were analyzed right after dialysis, after ageing at r. t. for 3 days and after annealing at 45ºC for one day. The representative TEM at pH 3 (a), 5.5 (b), 6 (c) and 8 (d) show that annealing reduces the morphological variety observed in freshly dialyzed samples (inserts). The difference is more pronounced at intermediate pH values where only patchy spherical particles are observed. The number of patches at pH 5.5 (e) and 7 (f) increases after annealing. Scale bars are 100 nm.

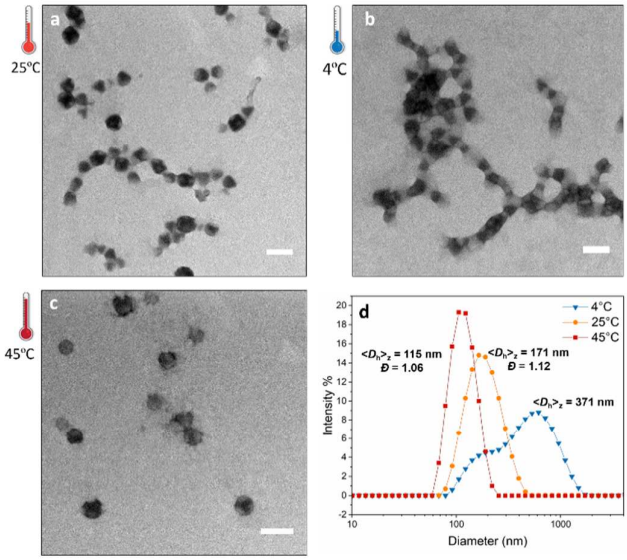

Fig. 7 Effect of temperature during self-assembly and ageing. Samples were dialyzed against 5 mM sodium acetate buffer at pH 6 for one day and aged for 3 days at different temperature. TEM micrographs at the end of the ageing process show that at moderately high temperature (45°C) only spherical patchy aggregates are formed (c) while at low temperature (4°C) "caterpillars" are still present even after ageing (b). DLS reflects the different size of the aggregates (d). Scale bars are 100 nm.

Elongated shape, compartmentalized core and glycosylated corona are very interesting features for a drug carrier mimicking a filovirus like ebola. For this reason, it is important to understand under which condition these structures can form and remain stable. In the following experiments we focus on self-assembly at pH 6, where caterpillar-type particles can be observed, and explore the effect of other variables. We already showed that a morphological transition to spherical aggregates occurs after annealing and, to some extent, after ageing the solution. Now we repeated the last step of the self-assembly process, dialysis against pH 6 acetate buffer for one day, at different temperature. The colloidal solutions were then aged for three days at the same temperature used for self-assembly and the morphology was analyzed by TEM (Fig. 7). When the primary particle solution in methanol/DMF 9:1 is dialyzed against pH 6 buffer solution (5 mM) at 4 °C, "caterpillars" are the predominant form of aggregation even after ageing. On the other hand, self-assembly and ageing at 45°C only produces spherical patchy aggregates and at room temperature the ageing process significantly reduces the "caterpillar" population in favor of spherical particles. Therefore, it is obvious that the caterpillar morphology can be kinetically selected and rendered stable for longer time with refrigeration, making it available for in vitro studies. This experiment shows that the system is very dynamic and even small temperature variations compared to the T_g of PBuA (-50°C) have a big effect on the stability of the aggregates.

Effect of concentration

According to the theory of hierarchical self-assembly, the mixed core/shell micelles (primary particles) undergo phase segregation upon dialysis against water and at the same time aggregate with each other to ensure the colloidal stability by minimizing interaction between the newly insoluble domain and the solvent.[18, 19] These two processes, segregation and aggregation, are interdependent and usually happen simultaneously. One strategy to isolate one from the other consists in crosslinking the core at the end of the assembly to produce a permanently segregated corona, incapable of mixing due to the inability of the core to rearrange.[19] We

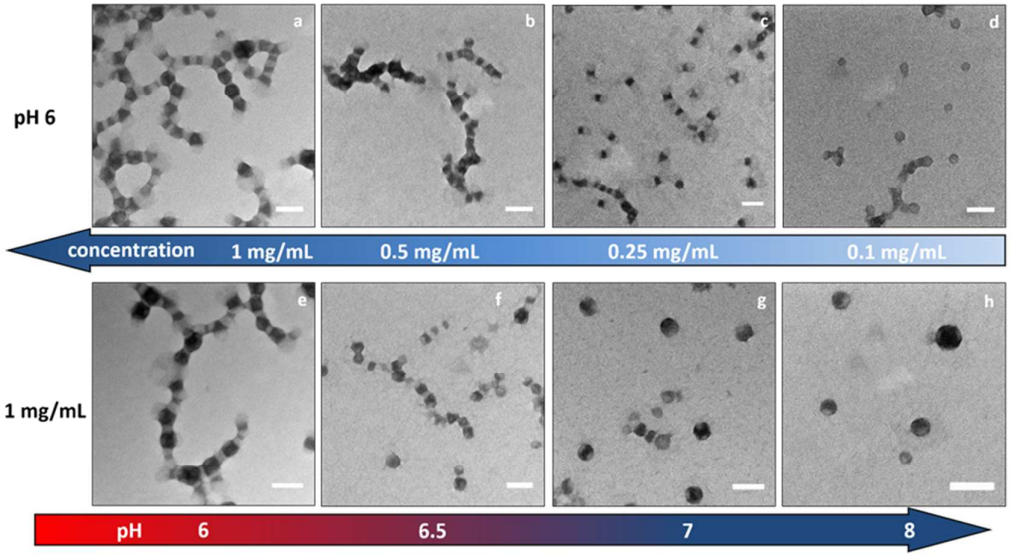

Fig. 8 Concentration-induced kinetic selection of the morphology during the higher level assembly of primary particles. At a constant pH of 6, a reduction in concentration of the primary particles solution reduces the tendency to aggregate and the 'caterpillar' morphology (a, b) is replaced by particles with 2 patches (c) or just one (d). A similar behavior to that observed before, with an increasing pH at a constant concentration of 1 mg/mL (e, f, g, h). Scale bars are 100 nm.

hypothesize that increasing or reducing the concentration in the second step of the self-assembly can increase or decrease the collision rate between primary particles and thus influence the aggregation towards linear assemblies or isolated spherical objects.

Diluting the primary particle solution with additional methanol had no effect on the particle size according to DLS measurements. These solutions at different concentration were dialyzed against pH 6 acetate buffer for one day at room temperature, like in the previous experiments. TEM analysis of the resulting aggregates right after dialysis is summarized in the top row of Fig. (see also Fig. S8†). We can see that when the concentration is relatively high (0.5 – 1 mg/mL) caterpillar-type aggregates with alternating domain represent the majority of the sample. When the concentration falls below 0.25 mg/mL, on the other hand, only very short "caterpillars" and particles with one or two patches can form. A higher concentration of 2 mg/mL still produced compartmentalized structures but had a negative effect on the colloidal stability of the solution can be observed (Fig. S8†; first column). DLS measurements show the same trend (Table S4†). If we assume that the segregation of the corona proceeds similarly for all samples, due to the same solvent exchange rate, then the morphological difference can be explained by a reduced collision rate between primary particles at low concentration. A low collision rate allows reorganization of the core and smaller aggregates have time to find colloidal stability. At very low concentration (0.1 mg/mL) the primary particles themselves can stabilize the insoluble P4VP block and aggregation is largely prevented. Supporting this hypothesis, once we concentrated the solution form 0.1 mg/mL to approximately 0.5 mg/mL in vacuo, the small particles do not form caterpillars or other big aggregates but remain small, stabilized by the hydrophilic corona (Fig S9†).

A similar trend is observed from the previous experiments (Fig. , Fig. bottom row). At a constant concentration of 1 mg/mL, a higher pH value and lower degree of ionization causes a faster segregation of the P4VP block from the corona to the core. Assuming a constant collision rate, the faster the segregation the smaller the resulting aggregate. This experiment demonstrates that in order to kinetically trap the caterpillar-type morphology it is necessary to optimize both pH value of the aqueous solution and concentration of the primary particle solution.

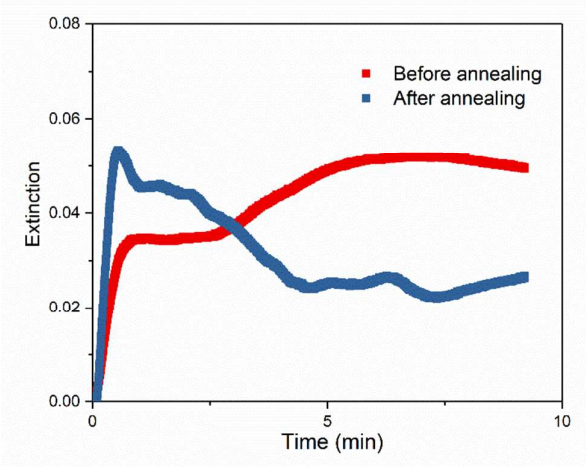

Fig. 9 Turbidity assay for the qualitative evaluation of ConA binding. The samples were dialyzed against pH 6 sodium acetate/acetic acid buffer (5 mM) and the assay was conducted before and after annealing. The annealed sample (patchy spheres) can crosslink the ConA solution faster than the sample before annealing (caterpillars).

Lectin binding

To confirm the availability of glucosyl functional groups on the surface of the nanoparticles it is relevant to evaluate their conjugation with lectins. While our aim is not to provide a detailed quantitative study on nanoparticle-lectin interactions, we conducted a qualitative evaluation using the turbidimetrey assay.[37-39] Concanavalin A (ConA) is a lectin with four binding pockets specific for glucosyl and mannosyl groups. Addition of glucose functionalized nanoparticles to a ConA solution increases the turbidity due to crosslinking between lectin molecules. In the assay the turbidity is monitored by UV-vis spectroscopy, measuring the extinction at 420 nm over time. The samples at pH 6 before and after annealing were used in representation respectively of "caterpillar" and patchy spherical morphologies. Both samples show an increase in turbidity upon addition to a ConA solution, indicating that their surface is indeed functionalized with bioactive glucose residues. The patchy spherical sample reaches its maximum extinction more quickly than the caterpillar-shaped one, indicating a more efficient crosslinking effect.

Conclusions

In summary we designed and synthesized a well-defined linear triblock glycopolymer PGlcEA-*b*-PBuA-*b*-P4VP, that can form various compartmentalized morphologies in aqueous solution through a hierarchical self-assembly process triggered by solvent exchange. Going from DMF to methanol to water we can successively collapse the B and C block and induce aggregation into more complex structures. The acidity of the solution is the main variable that determines the final morphology, as we anticipated, due to the pH-responsiveness of the P4VP block. Accurate control of the pH is crucial to direct the higher-level assembly. We can produce spherical particles without core compartmentalization, bigger particles with a phase-segregated patchy core, smaller aggregates with only few patches and linear caterpillar-type structures with alternating core domains. All these morphologies are obtained from a single polymer, only changing external conditions. In particular, the stability of the "caterpillar" morphology was investigated in detail and we found that even moderate temperature variation during and after self-assembly have a big impact on the stability of the aggregates. A lower temperature is beneficial to increase the stability of linear structures while a higher temperature favors spherical ones. Furthermore, a higher concentration of the primary particle solution in the second step of the self-assembly, promotes the formation of "caterpillars" over smaller spherical aggregates. We showed that the adaptation of the hierarchical self-assembly process to aqueous solution using bioactive polymers is possible provided that all external conditions are considered and optimized. Since applications in the biomedical

field only allow specific temperature and acidity, stabilization of hierarchical aggregates, for instance by crosslinking, is necessary to make these morphologies available as nanocarriers.

Conflicts of interest

There are no conflicts to declare.

Acknowledgements

The authors would like to acknowledge the UNSW Mark Wainwright Analytical Centre, in particular the NMR and EMU units.

References

1. G. Moad, E. Rizzardo and S. H. Thang, *Aust J Chem*, 2005, **58**, 379-410.
2. G. Moad, E. Rizzardo and S. H. Thang, *Polymer*, 2008, **49**, 1079-1131.
3. M. H. Stenzel, *Macromol. Rapid Commun.*, 2009, **30**, 1603-1624.
4. G. Moad, E. Rizzardo and S. H. Thang, *Aust J Chem*, 2012, **65**, 985-1076.
5. J. Li, H. Mao, N. Kawazoe and G. Chen, *Biomater. Sci.*, 2017, **5**, 173-189.
6. A. Blanazs, S. P. Armes and A. J. Ryan, *Macromol. Rapid Commun.*, 2009, **30**, 267-277.
7. J. Zhao, H. Lu, P. Xiao and M. H. Stenzel, *ACS Appl. Mater. Interfaces*, 2016, **8**, 16622-16630.
8. C. A. Fustin, V. Abetz and J. F. Gohy, *Eur. Phys. J. E*, 2005, **16**, 291-302.
9. A. O. Moughton, M. A. Hillmyer and T. P. Lodge, *Macromolecules*, 2012, **45**, 2-19.
10. A. Walther and A. H. Müller, *Chem. Commun. (Camb.)*, 2009, DOI: 10.1039/b820507h, 1127-1129.
11. A. H. Gröschel and A. H. Müller, *Nanoscale*, 2015, **7**, 11841-11876.
12. H. V. Berlepsch, C. Böttcher, K. Skrabania and A. Laschewsky, *Chem. Commun. (Camb.)*, 2009, **1**, 2290-2292.
13. S. Kubowicz, J. F. Baussard, J. F. Lutz, A. F. Thunemann, H. V. Berlepsch and A. Laschewsky, *Angew. Chem. Int. Ed. Engl.*, 2005, **44**, 5262-5265.
14. K. Skrabania, A. Laschewsky, H. V. Berlepsch and C. Böttcher, *Langmuir*, 2009, **25**, 7594-7601.
15. J. Marsat, M. Heydenreich, E. Kleinpeter, H. Berlepsch, V., C. Böttcher and A. Laschewsky, *Macromolecules*, 2011, **44**, 2092-2105.
16. H. Cui, Z. Chen, S. Zhong, K. L. Wooley and D. J. Pochan, *Science*, 2007, **317**, 647-650.
17. K. Kempe, R. Hoogenboom, S. Hoeppener, C. A. Fustin, J. F. Gohy and U. S. Schubert, *Chem. Commun. (Camb.)*, 2010, **46**, 6455-6457.
18. A. H. Gröschel, F. H. Schacher, H. Schmalz, O. V. Borisov, E. B. Zhulina, A. Walther and A. H. Müller, *Nat. Commun.*, 2012, **3**, 710.
19. A. H. Gröschel, A. Walther, T. I. Lobling, F. H. Schacher, H. Schmalz and A. H. Müller, *Nature*, 2013, **503**, 247-251.
20. E. Blanco, H. Shen and M. Ferrari, *Nat. Biotechnol.*, 2015, **33**, 941-951.
21. Y. Geng, P. Dalhaimer, S. Cai, R. Tsai, M. Tewari, T. Minko and D. E. Discher, *Nat. Nanotechnol.*, 2007, **2**, 249-255.
22. E. H. Miller and K. Chandran, *Curr. Opin. Virol.*, 2012, **2**, 206-214.
23. A. Walther, C. Barner-Kowollik and A. H. Müller, *Langmuir*, 2010, **26**, 12237-12246.
24. S. O. Kyerematen, K. Busse, J. Kohlbrecher and J. Kressler, *Macromolecules*, 2011, **44**, 583-593.
25. Y. Cao, N. Zhao, K. Wu and X. X. Zhu, *Langmuir*, 2009, **25**, 1699-1704.
26. A. Skandalis and S. Pispas, *Polym. Chem.*, 2017, **8**, 4538-4547.
27. D. J. Pochan, J. H. Zhu, K. Zhang, K. L. Wooley, C. Miesch and T. Emrick, *Soft Matter*, 2011, **7**, 2500-2506.
28. S. T. Li, X. He, Q. L. Li, P. F. Shi and W. Q. Zhang, *Acs Macro Lett.*, 2014, **3**, 916-921.
29. F. Huo, S. T. Li, Q. L. Li, Y. Q. Qu and W. Q. Zhang, *Macromolecules*, 2014, **47**, 2340-2349.
30. X. He, Y. Q. Qu, C. Q. Gao and W. Q. Zhang, *Polym. Chem.*, 2015, **6**, 6386-6393.
31. A. Dag, J. C. Zhao and M. H. Stenzel, *Acs Macro Lett.*, 2015, **4**, 579-583.
32. K. Babiuch, A. Dag, J. Zhao, H. Lu and M. H. Stenzel, *Biomacromolecules*, 2015, **16**, 1948-1957.
33. A. Dag, M. Callari, H. X. Lu and M. H. Stenzel, *Polym. Chem.*, 2016, **7**, 1031-1036.
34. J. Skey and R. K. O'Reilly, *Chem. Commun. (Camb.)*, 2008, **1**, 4183-4185.
35. S. Pearson, D. Vitucci, Y. Y. Khine, A. Dag, H. X. Lu, M. Save, L. Billon and M. H. Stenzel, *Eur Polym J*, 2015, **69**, 616-627.
36. M. Satoh, E. Yoda, T. Hayashi and J. Komiyama, *Macromolecules*, 1989, **22**, 1808-1812.
37. Y. Chen, G. Chen and M. H. Stenzel, *Macromolecules*, 2010, **43**, 8109-8114.
38. Y. Chen, M. S. Lord, A. Piloni and M. H. Stenzel, *Macromolecules*, 2015, **48**, 346-357.
39. K. N. R. Wuest, V. Trouillet, A. S. Goldmann, M. H. Stenzel and C. Barner-Kowollik, *Macromolecules*, 2016, **49**, 1712-1721.

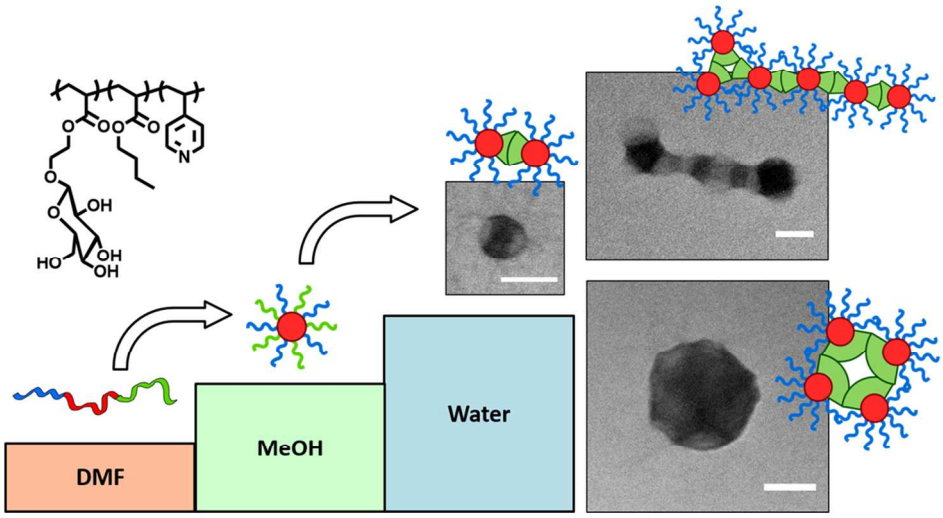

338x190mm (96 x 96 DPI)